
Modeling of γ -ray emission processes in Supernova Remnants

DESY Summer Student Programme, 2013

Leonardo Di Venere

Università degli studi di Bari, Italy

Supervisors

Elisa Bernardini

Rebecca Gozzini



2nd of September 2013

Abstract

In this work a C code to model the Spectral Energy Distribution (SED) of Supernova Remnants (SNRs) is developed. All the main non-thermal processes which produce photons are included. The model is then compared with data of a SNR and an algorithm based on χ^2 minimization is used to find the best fit values for the parameters of the model. Finally, the different steps which characterise the data analysis in MAGIC experiment are described.



Contents

1	Introduction	1
2	Supernova Remnants	2
3	Non-thermal photon production processes	2
3.1	Synchrotron emission	2
3.2	Inverse Compton Scattering	3
3.3	Bremsstrahlung radiation	4
3.4	Proton proton interaction	4
3.5	Spectral Energy Distribution	5
4	Code development and performance	5
4.1	Data fitting	6
4.2	An example: W51	7
5	MAGIC experiment and data analysis	7
6	Conclusion	10

1 Introduction

The first observation of particles coming from outer space (later on called cosmic rays) in 1912 by Victor Hess was the beginning of Astroparticle Physics. The subsequent observations of cosmic rays showed that they are composed mostly of protons, with a small percentage of heavier nuclei and electrons. The observed cosmic ray spectrum is represented in figure 1. The highest energy ever observed is approximately 10^{20} eV, an much higher energy than the typical energy reached in man-made particle accelerators ($\sim 10^{17}$ eV).

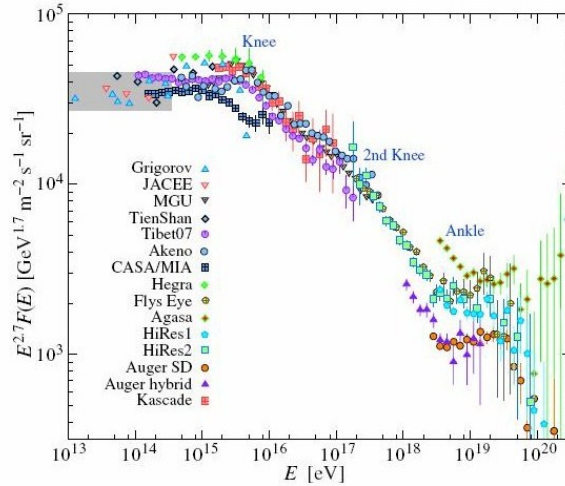


Figure 1: Observed cosmic rays spectrum. [1]

The energy spectrum is well described with a power law:

$$F(E) \propto E^{-s}. \quad (1)$$

The spectral index s is 2.7 up to the energy of about 10^{15} eV. Above this value, it becomes 3, corresponding to a steeper decrease of cosmic ray flux. This can be explained with the presence of some high energy particle sources, which accelerate particles up to the energy of 10^{15} eV (the "knee").

Cosmic rays do not give any information about their original source; the galactic magnetic field deflects and entraps them for a confinement time of about 10^6 years. Their trajectory is randomised and all the information about the source position is lost. However, these particles interact with the environment of their source and produce photons and neutrinos, which can travel to Earth without any deflection. This is why the detection of photons and neutrinos becomes fundamental to obtain information about the mechanisms accelerating particles at the source.

In this work, the mechanisms through which high energy particles produce photons are studied, from the radio energy band to very high energy γ -rays, focusing on a class of astrophysical objects, Supernova Remnants (SNRs). A model for the injection spectra of high energy particles is performed and it is then integrated with the cross sections of the photon production processes; the Spectral Energy Distribution of the SNR is then computed and fitted with data from different experiments, through a χ^2 minimisation algorithm.

2 Supernova Remnants

One of the possible galactic cosmic-ray accelerators are the Supernova Remnants (SNRs). A Supernova can be the final stage of a massive star. At equilibrium the gravitational force of the mass of the star is balanced by the fusion reactions in the core of the star, which involve mostly hydrogen. When the hydrogen in the star core is not sufficient to balance the gravitational force any more, heavier elements are formed through nuclear fusion and the star expands (red giant) losing the outer layers of gas. Finally, gravitational force prevails and the star collapses.

If the final mass of the star is larger than the Chandrasekhar limit ($1.4M_0$, with M_0 being the solar mass), the star ends its life as a Supernova. The gravitational force makes the star collapse and a hard core of neutrons is formed (neutron star). The collapsing star "bounces" on this hard neutron star and creates a shock wave that propagates far from the star. The shock wave can accelerate charged particles up to very high energy (10^{15} eV). The acceleration mechanism was proposed by E. Fermi and it predicts a power law spectrum for accelerated particles [2].

3 Non-thermal photon production processes

Accelerated electrons and protons interact with the SN environment and emit radiation through different mechanisms:

- Synchrotron emission, due to high energy electrons deflected in a magnetic field.
- Inverse Compton scattering of high energy electrons on low energy photons from the Cosmic Microwave Background (CMB), from infrared dust emission and from starlight.
- Bremsstrahlung radiation of high energy electrons accelerated in the Coulomb field generated by charged particles (electrons, protons and ions) of the gas surrounding the remnant.
- Decay of neutral resonances, produced in the interaction of high energy protons with target protons and ions present in the gas.

In the following sections, there is a simple description of these processes and the photon flux deriving from each process for a given differential injection spectrum for accelerated protons and electrons ($dN_p(E)/dE$ and $dN_e(E)/dE$ respectively) is evaluated. For a complete description see [3].

3.1 Synchrotron emission

The synchrotron emission occurs when electrons are deflected by a magnetic field. The spectrum of the emitted photons goes from the radio to the X-ray energy band, according to the strength of the magnetic field and to the electron energy.

A simple description of the phenomenon is given in [4].

The detailed calculation shows that the power emission formula from a single electron in a magnetic field B is given by:

$$\begin{aligned}
 P_e(\nu, \gamma, \theta) &= \frac{\sqrt{3}e^3 B \sin \theta}{mc^2} F(\nu/\nu_c) \\
 F(\nu/\nu_c) &= \frac{\nu}{\nu_c} \int_{\nu/\nu_c}^{\infty} K_{5/3}(y) dy \\
 \nu_c &= \frac{3}{2} \nu_s \sin \theta
 \end{aligned} \tag{2}$$

where θ is the angle that the velocity of the electron forms with the magnetic field (*pitch* angle) and $K_{5/3}(y)$ is the modified Bessel function of order 5/3.

In case of an isotropic emission (like in the case of SNRs), one can get rid of the angular factor by taking an average.

The specific emissivity (energy per unit solid angle and per unit frequency produced in a volume of 1 cm³) coming from many electrons is obtained by integrating the single electron emitted power multiplied by the differential injection spectrum:

$$\epsilon_s(\nu) = \int N(\gamma) P_e(\nu, \gamma) d\gamma. \quad (3)$$

An important characteristic of the resulting emissivity is that a power law electron distribution produces a power law emissivity spectrum and the two spectral indices are related. If α is the spectral index of the radiation and s the one of the injection, it can be demonstrated that

$$\alpha = \frac{s-1}{2}. \quad (4)$$

3.2 Inverse Compton Scattering

Inverse Compton scattering consists of the interaction of a high energy electron with a low energy photon; the electron transfers part of its energy to the seed photon, creating a γ -ray.

The cross-section of the process can be calculated using Feynman diagrams (see figure 2a). The result is given by the Klein-Nishina formula:

$$\sigma_{\text{KN}}(\gamma, \omega_0, \omega) = \frac{2\pi r_0^2}{\omega_0 \gamma^2} \left[1 + q - 2q^2 + 2q \ln(q) + \frac{\Gamma^2 q^2 (1-q)}{2(1+\Gamma q)} \right],$$

$$q = \frac{\omega}{4\omega_0 \gamma (\gamma - \omega)}, \quad (5)$$

$$(6)$$

where $\Gamma = 4\omega_0 \gamma$ and $\omega = h\nu/(mc^2)$; ω_0 is the corresponding quantity for the seed photon.

In the general case, seed photons are not monochromatic, but they are described by a density $n(\omega_0)$. For this reason, the previous cross-section must be integrated over all possible seed photons and all possible electrons, whose density is given by the injection spectrum:

$$\frac{dN_{\gamma, \text{IC}}}{dt d\omega} = \int d\omega_0 \int d\gamma \frac{dN_e(\gamma)}{d\gamma} n(\omega_0) \sigma_{\text{KN}}. \quad (7)$$

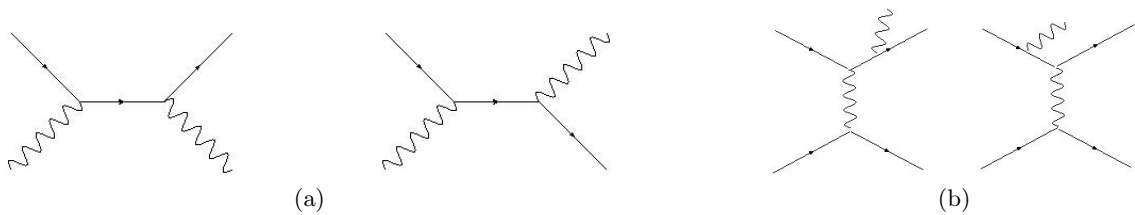


Figure 2: (a) Feynman diagrams for Inverse Compton Scattering. (b) Feynman diagrams for bremsstrahlung.

3.3 Bremsstrahlung radiation

When an electron interacts with the Coulomb field generated by charged particles, it radiates photons up to the γ -ray energy band. The process is described in Quantum Electrodynamics by the Feynman diagrams in figure 2b. Only the relevant diagrams have been considered, which are the ones where a high energy electron radiates a hard photon.

Bremsstrahlung of high energy electrons on target protons, electrons and helium nuclei was considered.

The cross-section of the process is given by the Bethe-Heitler formula for the electron-hadron interaction, while some relativistic corrections must be added for the electron-electron process [5]:

$$\begin{aligned}\sigma_{e-p}(\gamma, \omega) &= \sigma_1(\gamma, \omega), \\ \sigma_{e-e}(\gamma, \omega) &= (\sigma_1(\gamma, \omega) + \sigma_2(\gamma, \omega))A(\gamma, \omega),\end{aligned}\tag{8}$$

where σ_1 is the Bethe-Heitler formula in Born approximation, while σ_2 and $A(\gamma, \omega)$ contain the relativistic corrections for electron-electron bremsstrahlung (see the appendix in [5] for the detailed expressions).

The total photon rate is obtained by summing over the contribution of electron and ion bremsstrahlung. Only the contributions of Hydrogen ions (with density n_p), Helium ions (with density n_{He}) and electrons (with density n_e) are taken into account, with the assumptions $n_{\text{He}} = 0.1n_p$ and $n_e = 1.2n_p$. The target densities are assumed to be constant, which means that the integration over target density is straightforward. Finally, the integration over the electron energy (or its γ factor) is necessary to take into account the non-constant injection spectrum of electrons.

The final expression is:

$$\frac{dN_{\gamma, \text{brem}}}{dt d\omega} = \int d\gamma \frac{dN_e(\gamma)}{d\gamma} v_e ((n_p + 4n_{\text{He}})\sigma_{e-p}(\gamma, \omega) + n_e\sigma_{e-e}(\gamma, \omega)),\tag{9}$$

where v_e is the velocity of the incoming electron.

3.4 Proton proton interaction

The interaction between high energy protons and target protons is more difficult to describe. This process involves the interactions between quarks, which need Quantum Chromodynamics. In proton-proton deep inelastic scattering many neutral resonances are produced and they decay in 2 or more γ -rays. The most important contribution is π^0 decay:

$$p + p \rightarrow \pi^0 + X,$$

$$\pi^0 \rightarrow \gamma + \gamma$$

The analytical evaluation of the cross section of the process is not possible since QCD is involved. For this reason, the spectra of the resulting π^0 and consequently of γ -rays is simulated through some event generators (for example Pythia) and then parametrised with linear combinations of elementary function.

In this work, the parametrisation from Kelner, Aharonian and Bugayov ([6]) was used.

3.5 Spectral Energy Distribution

The photon flux described above is not usually compared directly to data. What is usually used is the energy flux or Spectral Energy Distribution (SED) of the source, which is obtained by multiplying the photon flux by the squared energy:

$$E^2 \frac{dN(E)}{dE}. \quad (10)$$

In the case of synchrotron radiation the corresponding quantity is:

$$\nu \epsilon_s(\nu). \quad (11)$$

The SED has the advantage that flattens a power-law with spectral index -2, so that a positive slope represents an index greater than -2, while a negative slope represents an index lower than -2.

4 Code development and performance

The evaluation of the contributions of the different processes must be done with a numerical integration of the cross sections. Starting from a template previously developed in Mathematica, a C code to evaluate the integrals numerically was developed in order to produce the values of the SED for a given set of initial parameters. The integrals were performed using the functions of the GNU Scientific Library (GSL) for numerical integration [7].

Regarding the injection spectrum, a broken power law with an exponential cutoff (used to ensure the convergence of all the integrals) was assumed both for protons and electrons:

$$N_{p/e}(E) = K_{p/e}/E_0 \frac{(E/E_0)^{-s}}{1 + (E/E_{br})^{ds}} \exp(-E/E_{cut}), \quad (12)$$

where $K_{p/e}$ is the spectrum normalization for proton and electrons respectively, s is the initial spectral index, ds is the change of the index at the break energy E_{br} , E_{cut} is the cut-off energy and E_0 is a scale energy fixed to the value of 1 GeV.

It must be noted that the initial spectral index must be the same for both protons and electrons, while all the other parameters can be different. In fact, s depends on the acceleration mechanisms only, which is the same for all particles (the mass difference is negligible, since ultra-relativistic particles are involved). On the contrary, the other parameters depend on the properties of the population of protons and electrons and there is no reason to assume they are the same.

With the normalisation chosen, the units of $K_{p/e}$ are [#photons/cm³]. However, in order to obtain the correct units for the final SED ([erg/(cm²s)]), the integrals must be multiplied by the volume in which each process is evolving (if an homogeneous emission is assumed) and the resulting flux must be rescaled by the distance of the source, i.e. divided by $4\pi d^2$, in order to obtain the actual flux measured on the Earth. These characteristics depend on the source under investigation and must be estimated *a priori* in order to compare the results obtained from different sources, since the normalisation derived from the SED analysis contains both the intrinsic normalisation of the injection particles and the re-scaling factors (emitting volume and distance).

For simplicity, in the following example, the emitting volumes are assumed to be the same for all the processes and all the re-scaling factors are set equal to 1.

As for the Inverse Compton scattering, seed photons from 3 different populations (one for CMB, one for infrared thermal emission and one for starlight) are considered. In all cases

a black body spectrum is assumed, which in the case of CMB is strictly valid, while for the other cases it is an approximation. The value of the typical temperature is fixed for the CMB ($T_{\text{CMB}} = 2.725\text{K}$); in the other two cases, the user must estimate the optimal temperature from other information. Moreover, in the case of infrared and optical emission, the spectra can be renormalised through the constants $A_{\text{norm,IR}}$ and $A_{\text{norm,opt}}$, in order to modify the relative weights of the three contributions.

Regarding the performance of the code, the most demanding process is the Inverse Compton, since it involves a double integration (first on seed photon spectrum and then on electron spectrum), and it takes most of the total computational time. The three components of the seed photons (CMB, infrared and optical) are evaluated separately, which means that each component takes about a third of the total time. For this reason, if there are some hints to say that the Inverse Compton scattering is much less important than the other two competitors (bremsstrahlung and $p-p$ interaction), it can be excluded from the model, with a high improvement in the code performance.

4.1 Data fitting

Having a model for the SED of a given SNR, a fit to this model with experimental data has to be done, in order to infer some information about the source itself and its environment. Since the model covers all the electromagnetic spectrum (from radio to γ -ray), data from different experiments have to be used.

In particular, data in the radio and X-ray energy band give information about the synchrotron emission, while the other three processes contribute to high energy γ -ray and very high energy γ -ray energy band (from 100 MeV up to 10 TeV).

A summary of the relevant parameters for each process is shown below:

- **Synchrotron emission:** injection parameters of electrons (in particular, spectral index and normalisation) and magnetic field.
- **Inverse Compton scattering:** injection parameters of electrons.
- **Bremsstrahlung radiation:** injection parameters of electrons, target electron, proton and ion density.
- **Proton Proton interaction:** injection parameters of protons, target proton density.

The fit was developed in the code, using a χ^2 -minimisation algorithm. The minimisation was implemented using the Levenberg-Marquardt method, which combines the inverse-Hessian method and the steepest descent method; the latter is used far from the minimum, switching continuously to the former when approaching the minimum (see [8] for more details). This method works for functions expressed as the sum of squares of non-linear functions, like the χ^2 of our model. A first guess for the initial values of the parameters is necessary to be able to perform the correct fit (in a reasonable time).

The algorithm was implemented in the code using the C library *levmar*, developed by M. Lourakis (see [9] for the documentation). This library takes the function to be fitted (the SED model), an initial guess for the parameters and the data points as inputs and finds the best fit values for the parameters through the minimisation of the associated χ^2 . Constraints were put on the parameters, limiting the range in which to find the minimum. These ranges are used to avoid the parameters to have non-physical values.

4.2 An example: W51

The fit code was tested on the data from the SNR W51C sited in the complex W51. Data in the different energy ranges were taken from different experiments. To the 21 cm radio continuum measurements [10], Fermi-LAT [11] (ApJL, 706 (2009)) and MAGIC measurements [12] in the γ -ray energy band were added.

A first guess was made by changing the parameters values manually. These values were then used as first guesses for the minimisation algorithm. The result of the fit was a table with the optimised values for the parameters and the relative χ^2 .

Two different fits were performed using different sets of initial values. In figure 3 the results are shown. In figure 3a the dominant process is the p-p interaction, with an inverse Compton contribution at very high energy. In figure 3b bremsstrahlung prevails with the p-p interaction giving a contribute of about 30% to the total. In table 1 there are the values of the model parameters before and after the fit. As for the Inverse Compton component, only the CMB contribution was taken into account for both cases.

It is interesting to point out how the results of the fit depend on the initial values. The human action becomes fundamental to decide whether the results are correct or not.

	Inverse Compton dominant fit $\chi^2/dof = 5.1/12$		Bremsstrahlung dominant fit $\chi^2/dof = 8.4/12$	
	Initial values	Best fit	Initial values	Best fit
s	1.5	1.47	1.5	1.34
$K_e(\text{GeV}^{-1} \text{ cm}^{-3})$	$1.0 \cdot 10^4$	$4.971 \cdot 10^3$	$1.0 \cdot 10^4$	$6.93 \cdot 10^3$
$K_p(\text{GeV}^{-1} \text{ cm}^{-3})$	$4.0 \cdot 10^7$	$4.47 \cdot 10^7$	$4.0 \cdot 10^5$	$2.75 \cdot 10^5$
ds_e	1.2	0.46	1.2	1.97
ds_p	1.0	1.50	1.0	1.27
$E_{br,e}(\text{eV})$	$1.0 \cdot 10^{10}$	$2.95 \cdot 10^{10}$	$1.0 \cdot 10^{10}$	$5.93 \cdot 10^9$
$E_{br,p}(\text{eV})$	$8.0 \cdot 10^9$	$1.50 \cdot 10^{10}$	$8.0 \cdot 10^9$	$4.93 \cdot 10^9$
$E_{cut,e}(\text{eV})$	$1.0 \cdot 10^{13}$	$5.31 \cdot 10^{12}$	$1.0 \cdot 10^{13}$	$1.26 \cdot 10^{13}$
$B(G)$	$1.0 \cdot 10^{-6}$	$7.84 \cdot 10^{-4}$	$1.0 \cdot 10^{-6}$	$5.42 \cdot 10^{-4}$
$n_p(\text{cm}^{-3})$	10.0	4.40	$1.0 \cdot 10^3$	$8.74 \cdot 10^2$

Table 1: Values of parameters of the model before and after the χ^2 minimisation for both the Inverse Compton dominant fit (left) and the bremsstrahlung dominant fit (right).

5 MAGIC experiment and data analysis

The last part of the project consisted in learning of data analysis procedure for the MAGIC experiment.

MAGIC is one of the experiments which can measure γ -rays with energy above 50 GeV. In this energy range, direct measurement of the photons with a space telescope (like in Fermi-LAT experiment) is not possible, since the low flux of these photons would require a too large effective area of the telescope. For this reason, the Earth's atmosphere is used as a target for the incoming high energy photons: when a γ -ray enters the atmosphere, it will interact with atoms and molecules and produce an electromagnetic shower, consisting of a number of relativistic electrons and positrons. These very high energy particles travel at a speed ($\approx c$) greater than the speed of light in the atmosphere and emit Cherenkov light (visible and UV light), which we can detect (Imaging Atmospheric Cherenkov Telescopes, IACT).

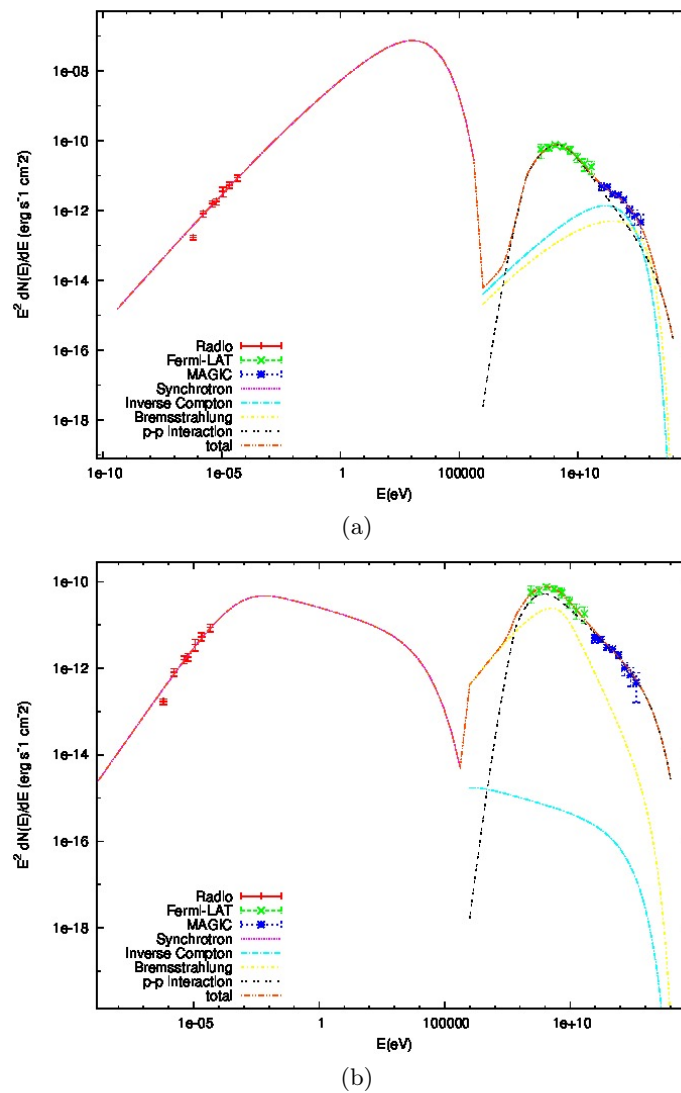


Figure 3: (a) Inverse Compton dominant fit. (b) Bremsstrahlung dominant fit.

MAGIC is an array of two telescopes, whose mirrors focus the faint Cherenkov light coming from electromagnetic showers on a camera of photomultipliers. From the shower image generated in the camera, the incoming photon characteristics (like energy, direction, etc.) are reconstructed. The most important characteristics of the telescopes are summarized in table 2.

MAGIC telescopes are equipped with a hardware stereo trigger. The first level of trigger is based on a simple pixel counting; an event is recorded only if a sufficiently high number of near pixels (3-4) give the signal in a pre-defined time window (≈ 10 ns). The stereo trigger combines the information from both the telescopes and validates only the events recorded by both telescopes. Later, the event is calibrated, cleaned from all spurious signals (isolated pixels in the camera) and parametrised, before being available for the analyser.

The procedure to reconstruct the event consists of different steps, which are performed through the MAGIC Software MARS. The most important steps are described below.

The first selection of data is done manually by the analyser. The runs (approximately 20 minutes each) or sub-runs (approximately 1 minute each) presenting some anomalies are removed from data. The next step consists in combining data from both telescopes and performing a first

Energy range	50 GeV - 10 TeV
Energy resolution	17% at ≈ 300 GeV
Sensitivity	0.8% Crab in 50h at ≈ 300 GeV
Angular resolution	0.07° at ≈ 300 GeV
Field of view	3.5°

Table 2: Some characteristics of the MAGIC Telescopes

geometric reconstruction of the arrival direction of the incoming particle; this is possible thanks to the stereoscopic view given by the combination of two telescopes.

The next step is the actual reconstruction of the event, consisting of three steps: energy reconstruction, arrival direction reconstruction and γ -hadron separation. The last step is the actual signal/background separation, where the signal consists of the photons, while the background is made of all other charged particles which produce electromagnetic showers (mostly cosmic-ray protons).

- **Arrival direction.** The reconstruction of the arrival direction is performed with two independent methods. The first is based only on the geometry of the shower image, which is parametrised with an ellipse; the combination of the directions of the ellipse axes from both the telescopes gives the direction of the incoming photon. The second is applied to the two telescopes separately, but it needs some Monte Carlo simulations. The Distance Image Source Position (DISP) parameter, which is the angle between the γ -ray source and the shower max direction, is estimated through a previously trained Random Forest. Sometimes, two positions for the source are allowed, due to the symmetry of the image. The final reconstruction is performed by combining the information from the two telescopes. The parameters of the images are then re-calculated taking into account the new reconstructed direction.
- **Energy.** The energy reconstruction is based on comparing the characteristics of the detected event with the ones of a simulated event. Look-up tables are built through a simulation software (like CORSIKA [13]) and then compared to the detected events.
- **γ -hadron separation.** This step is the actual signal/background separation. It is based on a Random Forest (RF) algorithm. The characteristics of the event are used to build the decision trees of the RF, which have to be trained using some Monte Carlo events. As a result, each event will be characterised by a new parameter, the *hadroness*, which tells the probability of the event to be a photon or a hadron.

Now the reconstructed events are ready to be combined together to infer some physical information about the region under consideration. Three are the main tools used to perform this part of the analysis.

- **Signal significance.** A θ^2 plot is produced, where θ is the angle between the pointed direction and the incoming photon direction; it gives information about the presence of signal (a peak for $\theta = 0$ is expected) and its significance, depending on the number of the number of signal events with respect to the irreducible background events, consisting of the residual cosmic ray hadrons. This background can be extrapolated by some measurements performed contemporary to the signal measurements in a different region of the camera (Wobble technique).

- **Sky maps.** Sky maps of the observed region are created (usually in RA e DEC coordinates), by counting the number of events for each bin of the observed region. They can be used to infer information about the shape and extension of the source (if its dimensions are greater than the instrument Point Spread Function, i.e. how large a point source appears) and eventually subtract the contribution of other sources in the field of view of the telescopes.
- **Flux.** A calculation of the differential flux of the source, i.e. the number of photons per unit time, unit area and per energy bin, is performed. An evaluation of the exposure time and of the effective area of the telescopes must be done and Monte Carlo simulations are used once more. Light curves, representing the time variation of the integrated flux, are also calculated.

6 Conclusion

The modeling of Supernova Remnants SED is important to get information about the particle population and the processes characterising the source. The code developed in this work is a powerful tool to evaluate the photon spectra coming from non-thermal emission of the processes discussed above. This model is then fit to data. However, given the relative high number of free parameters (~ 10), the first guess of the parameters is important for the correct convergence of the fit.

Moreover, additional information about the free parameters of the fit are still necessary for the correct interpretation of the result and to avoid non-physical results.

Acknowledgements

First of all, I would like to thank both my supervisors, Elisa Bernardini for the precious suggestions she gave me, even in the few conversations we had, and Rebecca Gozzini for her everyday support and her patience in answering all of my questions. Thanks also to Gessica De Caneva for being my third supervisor and for her help in the last part of my work.

A special thank to Karl Jansen for the great coordination of the programme and all his efforts to make us feel comfortable here.

Finally, I am very grateful to my supervisor in my university in Bari, Francesco Giordano, for his constant encouragement and support and for all the advice he has given me during the last year.

References

- [1] *Review of Particle Physics* edited by Particle Data Group, Physics Letters, **B667**, (2008) 1 "24. Cosmic Ray"
- [2] Fermi E., *On the Origin of the Cosmic Radiation*, Physical Review, **75**, 1169-1174 (1949).
- [3] G. R. Blumenthal, R. J. Gould, *Bremsstrahlung, Synchrotron Radiation, and Compton Scattering of High-Energy Electrons Traversing Dilute Gases*, Reviews of Modern Physics, **42**, 237 (1970).
- [4] G. Ghisellini, *Radiative Processes in High Energy Astrophysics*, arXiv:1202.5949v1 (2012).

-
- [5] M. G. Baring et al., *Radio to Gamma-ray Emission from shell-type Supernova Remnants: predictions from non-linear shock acceleration model*, The Astrophysical Journal, **513**, 311 (1999).
- [6] S. R. Kelner, F. A. Aharonian, V. V. Bugayov, *Energy spectra of gamma rays, electrons, and neutrinos produced at proton-proton interactions in the very high energy regime*, Phys. Rev. D, **74**, 034018 (2006).
- [7] *GNU Scientific Library*, <http://www.gnu.org/software/gsl/>
- [8] W. H. Press, S. A. Teukolsky, W. T. Vetterling, B. P. Flannery, *Numerical Recipes, 3rd Ed.* (Cambridge University Press, 2007).
- [9] M. Lourakis, *levmar*, <http://users.ics.forth.gr/~lourakis/levmar/>
- [10] B. Koo and D. Moon, *Interaction between the W51C Supernova Remnant and a Molecular Cloud. I. H I 21 Centimeter Line Observations*, Astrophysical Journal, **475**, 194 (1997).
- [11] A. A. Abdo et al., *Fermi-LAT Discovery of Extended Gamma-Ray Emission in the Direction of Supernova Remnant W51C*, The Astrophysical Journal, **706**, L1–L6 (2009).
- [12] J. Aleksić et al., *Morphological and spectral properties of the W51 region measured with the MAGIC telescopes*, Astronomy and Astrophysics, **541**, A13 (2012).
- [13] *CORSIKA*, <http://www-ik.fzk.de/~corsika/>